

Electronic Supplementary Information for

## Facile Synthesis of Supported CuNi Nano-clusters as Electrochemical CO<sub>2</sub> Reduction Catalyst with Broad Potential Range

Jiale Wang,<sup>a</sup> Fan Li,<sup>a</sup> Runhua Li,<sup>a</sup> Qian Xiang,<sup>a</sup> Wencong Zhang,<sup>a</sup> Chengyi Song,<sup>a</sup> Peng Tao,<sup>a</sup> Wen Shang,<sup>a</sup> Tao Deng,<sup>a,b</sup> Hong Zhu,<sup>a,c,d</sup> and Jianbo Wu\*,<sup>a,b,d,e</sup>

<sup>a</sup> State Key Laboratory of Metal Matrix Composites, School of Materials Science and Engineering,  
Shanghai Jiao Tong University, Shanghai 200240, China

<sup>b</sup> Center of Hydrogen Science, Shanghai Jiao Tong University, Shanghai 200240, China

<sup>c</sup> University of Michigan-Shanghai Jiao Tong University Joint Institute, Shanghai 200240, China

<sup>d</sup> Materials Genome Initiative Center, Shanghai Jiao Tong University, Shanghai 200240, China

<sup>e</sup> Future Material Innovation Center, Zhangjiang Institute for Advanced Study, Shanghai Jiao Tong  
University, Shanghai, 200240, China.

\*To whom correspondence should be addressed. E-mail: jianbowu@sjtu.edu.cn

## Experimental Section

### Synthesis of ZIF-8

Typically, 6.4g 2-methylimidazole (MeIM) and 2.97g zinc nitrate hexahydrate ( $\text{Zn}(\text{NO}_3)_2 \cdot 6\text{H}_2\text{O}$ ) were dissolved in 50 mL methanol, respectively. Then, the solution of MeIM was added into  $\text{Zn}(\text{NO}_3)_2$  solution rapidly and stirred for 2 h at room temperature (700 rpm). After the reaction, the precipitate was obtained by centrifugation (6000 rpm, 8 min) and washed with ethanol three times. Finally, the obtained precipitate was dried in vacuum at 60°C for about 8 h.

### Synthesis of CuNi-ZIF, Ni-ZIF, and Cu-ZIF

To obtain CuNi-ZIF, 2g nickel nitrate hexahydrate ( $\text{Ni}(\text{NO}_3)_2 \cdot 6\text{H}_2\text{O}$ ) and 1.25g cupric acetate anhydrous ( $\text{Cu}(\text{CH}_3\text{COO})_2$ ) were dissolved in 20mL deionized water, respectively. 100 mg obtained ZIF-8 was dissolved in 12 mL n-hexane and stirred for 5 minutes. Then, 25  $\mu\text{L}$  as-prepared  $\text{Ni}(\text{NO}_3)_2$  and  $\text{Cu}(\text{CH}_3\text{COO})_2$  solution were added into the ZIF-8 solution separately and stirred for 3h. The precipitate was obtained by centrifugation (1000 rpm, 5min) and then dried in vacuum at 60°C for about 8 h. The synthesized procedures of Ni-ZIF and Cu-ZIF were the same as the CuNi-ZIF, except for 50  $\mu\text{L}$   $\text{Ni}(\text{NO}_3)_2$  solution for Ni-ZIF and 50  $\mu\text{L}$   $\text{Cu}(\text{CH}_3\text{COO})_2$  solution for Cu-ZIF.

### Synthesis of CuNi-NC, Ni-NC, Cu-NC

To get CuNi-NC, the as-obtained CuNi-ZIF was placed in a tube furnace and heated to 1000°C for 2 h under the Ar atmosphere; the heating rate was 5°C min<sup>-1</sup>. Then, with the same method, Ni-ZIF and Cu-ZIF were used to synthesize the Ni-NC and Cu-NC.

### Synthesis of CuNi-NC-0.5h and CuNi-NC-1h

To get CuNi-NC-0.5h and CuNi-NC-1h, the as-obtained CuNi-ZIF was placed in a tube furnace and heated to 1000 °C for 0.5 h and 1 h in Ar atmosphere; the heating rate was 5°C min<sup>-1</sup>.

### Characterization

Transmission electron microscopy (TEM) and selected area electron diffraction (SAED) were carried out on JEOL-2100F. High-angle annular dark-field scanning TEM (HAADF-STEM) and Elemental mapping were carried out JEOL JEM-ARM200F S/EM. XRD was performed on a LabX XRD-6100 Shimadzu with a scanning range of 10° ~ 80° by the scan rate of 5° min<sup>-1</sup>. Raman spectra data were obtained by Renishaw inVia Qontor spectroscopy system. Nitrogen adsorption-desorption isotherms and pore size distributions were measured with the equipment of BELSORP-MAX. Elemental content analysis of Ni and Cu in power samples was detected by inductively coupled plasma (ICP) spectrometry (iCAP6300). XPS results were recorded by Thermo ESCALAB250i.

### Electrochemical Measurements

The electrochemical measurements were performed in an H-cell, which was separated by a cation exchange membrane and recorded via the equipment of CHI760E. Pt foil was used as the counter electrode, and the Ag/AgCl electrode was used as the reference electrode. To make the working electrode, the ink was prepared with a 5 mg catalyst and 40  $\mu\text{L}$  Nafion, and 1 mL isopropanol. Then, 100 $\mu\text{L}$  formulated ink was dropped on carbon paper and dried in air. The loading amount of the catalyst was 1 mg/cm<sup>2</sup>. CO<sub>2</sub>-saturated 0.1 M KHCO<sub>3</sub> (pH=6.8) aqueous solution was used as the electrolyte. All potentials were calculated with respect to the reversible hydrogen electrode (RHE), which were converted according to the Nernst equation:  $E_{\text{vs RHE}} = E_{\text{vs Ag/AgCl}} + 0.059 \times \text{pH} + 0.199 \text{ V}$ . Linear sweep voltammetry was performed with a scan rate of 10 mV s<sup>-1</sup>. **All electrochemical tests were carried out without iR compensation.**

The gaseous products were quantified by a gas chromatograph (GC) equipped with a flame ionization detector (FID) and a thermal conductivity detector (TCD). Highly pure N<sub>2</sub> (99.999%) was used as the carrier gas. Electrochemical impedance spectroscopy (EIS) was measured with a range of 0.1 Hz to 0.1 M Hz. The electrochemical active surface area (ECSA) test was measured by operating cyclic voltammetry (CV) at different scanning rates (5, 10, 15, 20, 25, 30 mV s<sup>-1</sup>).

TOF for CO production was calculated as follows:

$$TOF (h^{-1}) = \frac{I_{CO}/nF}{m_{cat} \times w/M_{metal}} \times 3600$$

$I_{CO}$ : partial current of CO, A;

$n$ : the number of electrons transferred for CO production, which is 2 for CO;

$F$ : Faradaic constant, 96485 C mol<sup>-1</sup>;

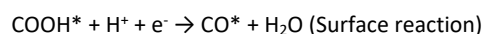
$m_{cat}$ : the mass of catalyst on the electrode, g;

$w$ : the metal loading in the sample measured by ICP;

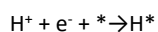
$M_{metal}$ : relative atomic mass of metal.

### DFT calculations

Density functional theory (DFT) calculations based on the projector augmented wave (PAW) method<sup>1</sup> were carried out by utilizing the Vienna ab initio simulation package (VASP)<sup>2, 3</sup> with the generalized gradient approximation (GGA),<sup>4</sup> the Perdew-Burke-Ernzerhof (PBE) exchange-correlation functional in the treatment of electron-ion interactions and cut-off energy of 520 eV for a plane wave expansion of the wave functions. A (3×3) surface cell model was constructed to express (111) surface of CuNi/C, Cu/C, and Ni/C. The CuNi/C structure was constructed by substituting the Ni atom with the Cu atom in all possible geometries and selecting the most stable one.<sup>5</sup> The Monkhorst-Pack grid of size of 1×1×1 was adopted to sample the CuNi/C, Cu/C, and Ni/C surface Brillouin zone.<sup>6</sup> A vacuum region of 15 Å was added to give converged adsorption energies while the energy convergence criterion is 0.0001 eV/atom for electronic minimization steps. It is well known that the whole process of CO<sub>2</sub> electrochemical reduction to CO mainly includes the following three steps.<sup>7, 8</sup> Gibbs free energy for each step of these slabs was calculated.



Considering that the adsorption free energy of intermediate hydrogen,  $\Delta G_{H^*}$ , was used as a descriptor to evaluate the electrocatalytic activity of HER,<sup>9</sup> we also calculated  $\Delta G_{H^*}$  of these three slabs to explain their HER activity. The Sabatier principle indicated that the moderate hydrogen adsorption, that is  $\Delta G_{H^*} = 0$ , gives the optimal HER activity.<sup>10</sup> For the HER process in this work, we consider the following steps and Gibbs free energy for each step of all slabs was calculated.



The calculating method for UL was as follows:

$$U_L = -\frac{\Delta G}{e}$$

$\Delta G$ : the lowest energy required to make all reaction steps downhill in free energy.

$e$ : unit electron.

## Results and Discussion

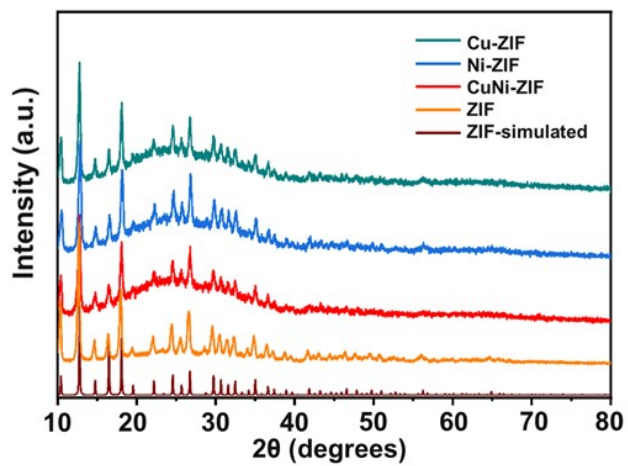


Fig. S1 XRD patterns of the simulated ZIF-8, ZIF-8, Cu-ZIF, Ni-ZIF, and CuNi-ZIF.

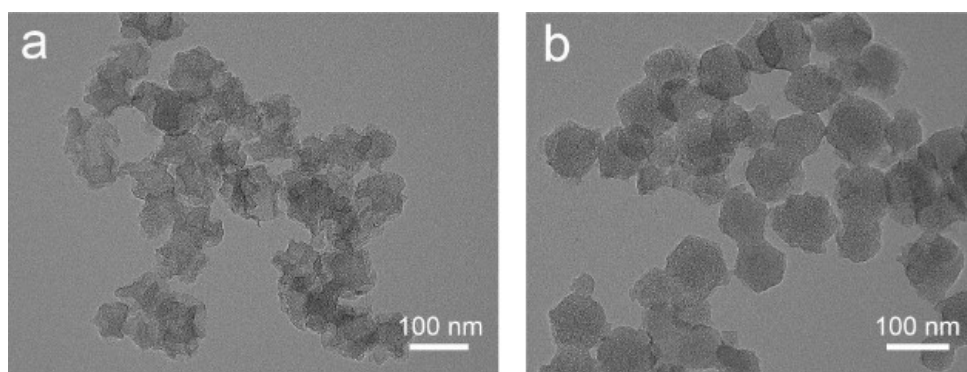
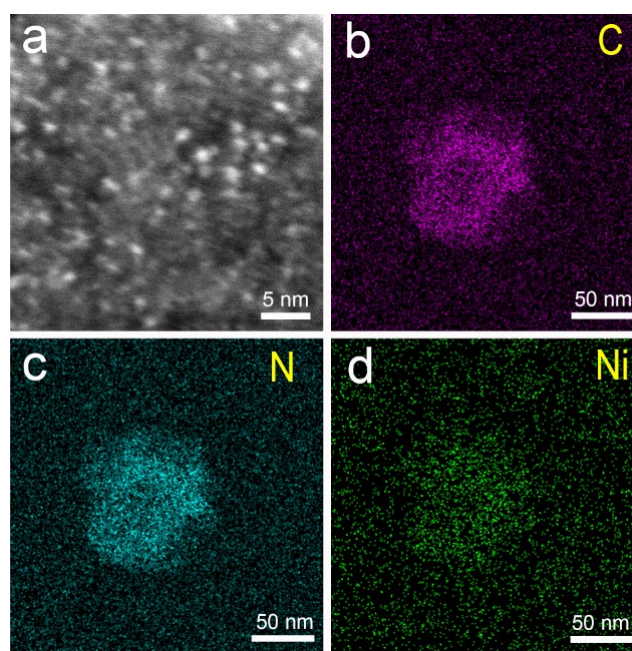
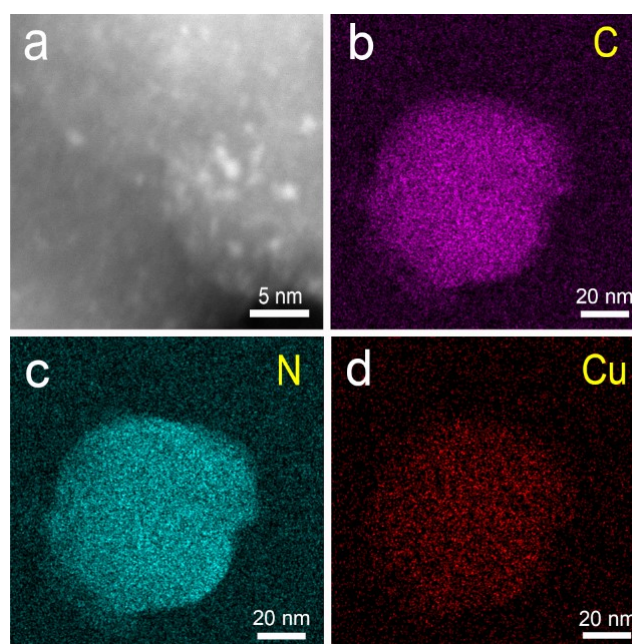


Fig. S2 TEM images of the (a) Ni-NC and (b) Cu-NC.



**Fig. S3** HAADF-STEM images (a) and corresponding elemental mapping of Ni-NC: (b) C, (c) N, (d) Ni.



**Fig. S4** HAADF-STEM images (a) and corresponding elemental mapping of Cu-NC: (b) C, (c) N, (d) Cu.

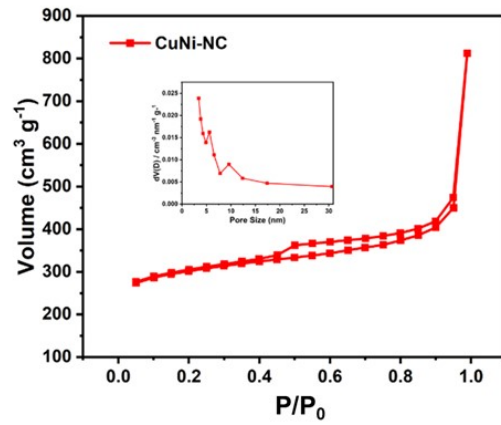


Fig. S5 N<sub>2</sub> absorption isotherms of CuNi-NC, inset image corresponding to the pore size distribution.

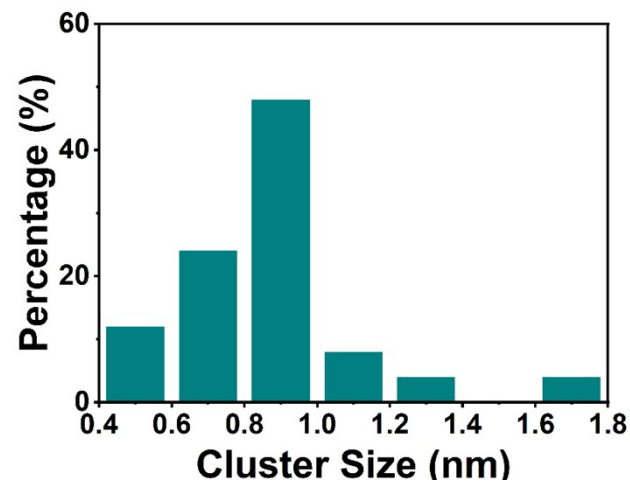
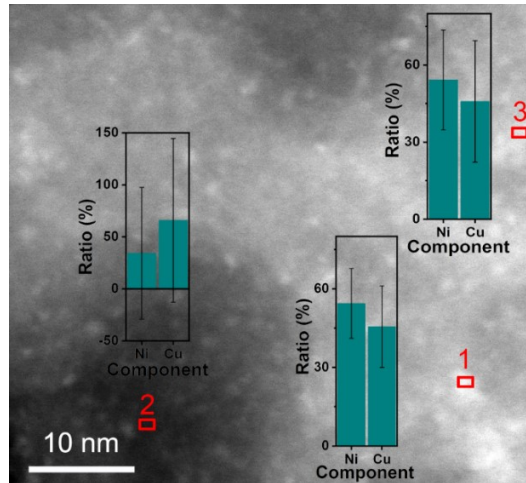
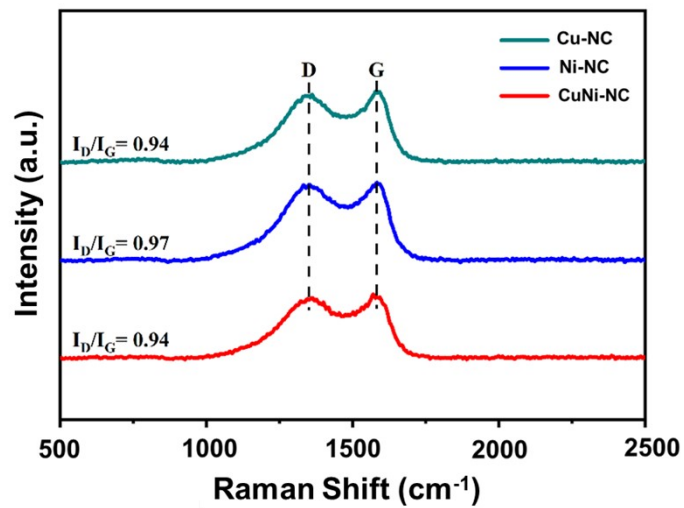


Fig. S6 Bimetallic cluster size distribution of CuNi-NC



**Fig. S7** The ratio of Cu and Ni in regions 1, 2, and 3 by EDS. Regions 1 and 3 on the bimetallic cluster show the content of Ni is close to Cu, while region 2 is beyond the cluster and indicates the absence of Ni and Cu.



**Fig. S8** Raman spectra of CuNi-NC, Ni-NC, and Cu-NC.

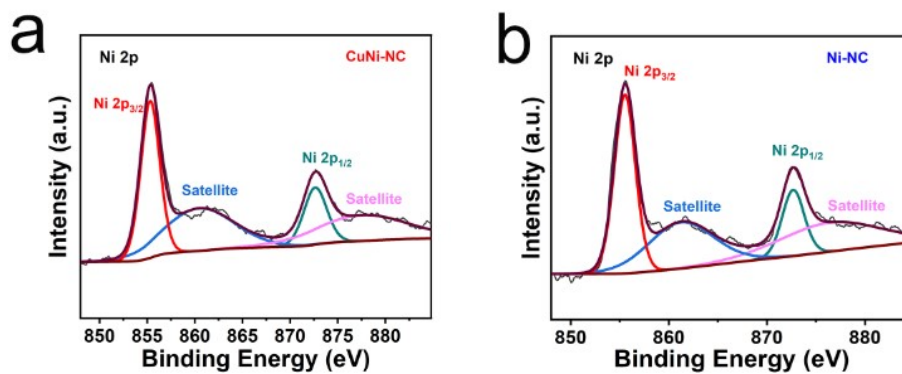


**Fig. S9** XPS spectra of Ni 2p in (a) CuNi-NC, (b) Ni-NC.

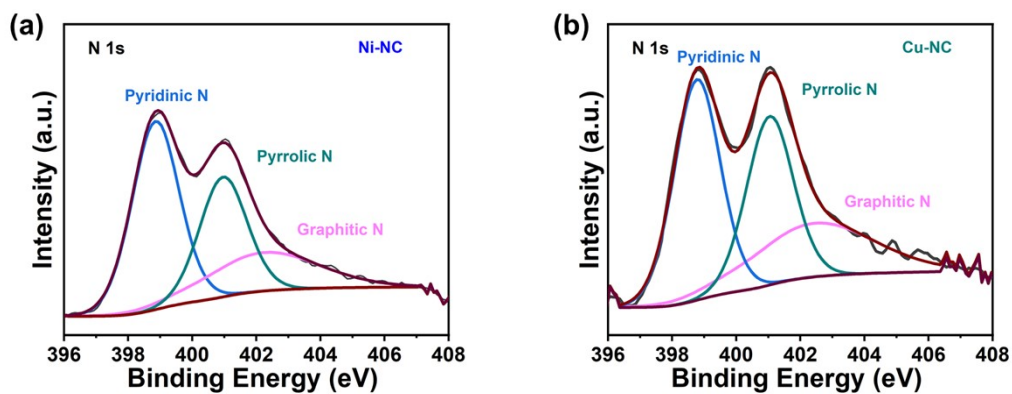


Fig. S10 XPS spectra of N 1s in (a) Ni-NC, (b) Cu-NC.

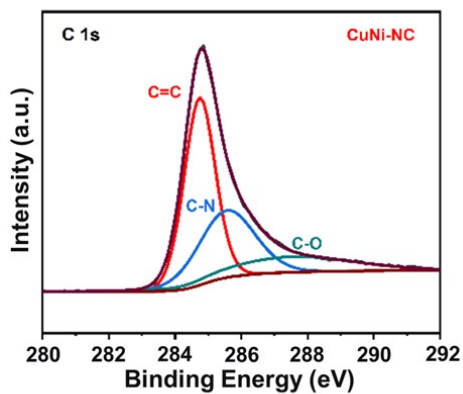


Fig. S11 XPS spectra of C 1s in CuNi-NC.

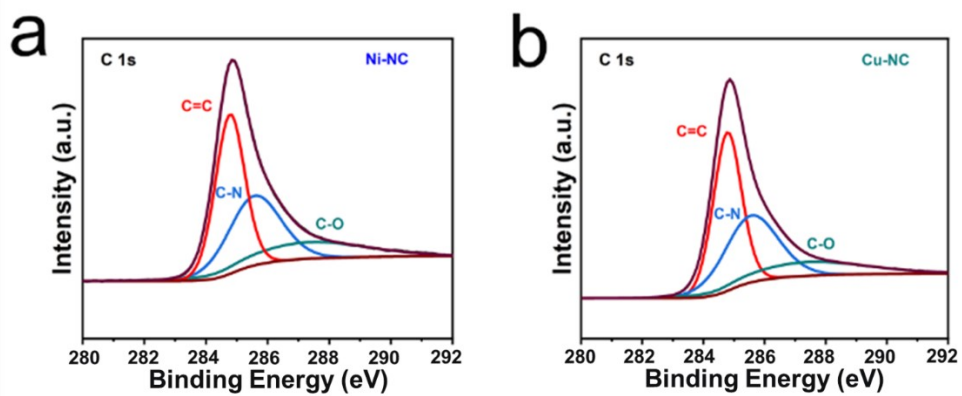
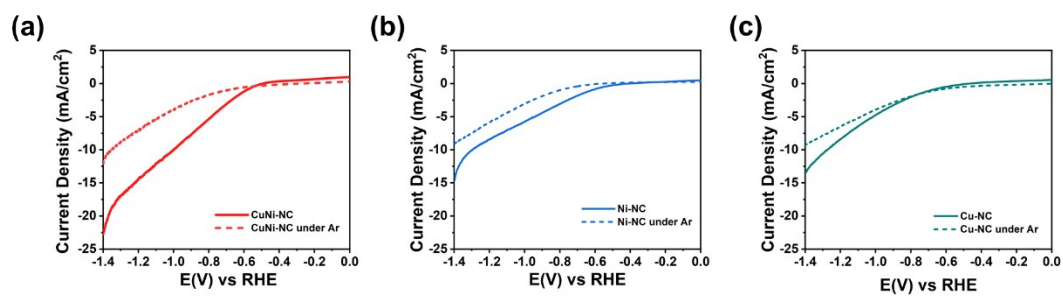
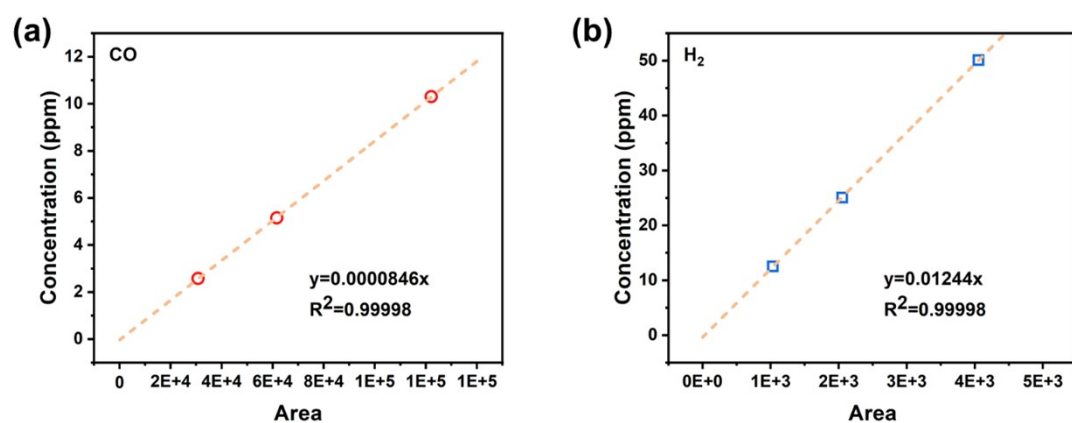


Fig. S12 XPS spectra of C 1s in (a) Ni-NC, (b) Cu-NC.



**Fig. S13** Comparisons of LSV curves in CO<sub>2</sub>-saturated (solid line) and Ar-saturated (dash line) electrolyte: (a) CuNi-NC; (b) Ni-NC; (c) Cu-NC.



**Fig. S14** GC calibration curves for (a) CO and (b) H<sub>2</sub>.

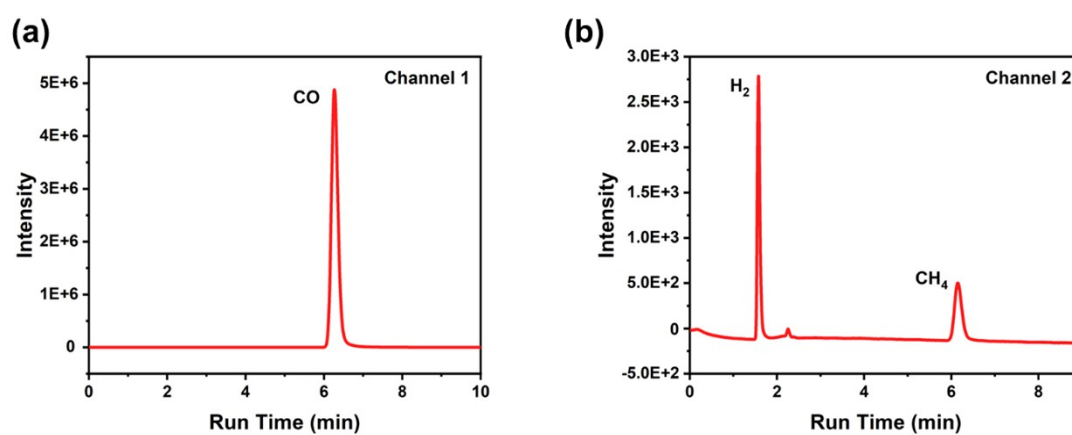


**Fig. S15** A typical data plot of GC for CuNi-NC electrolyzed at -1.0 V vs RHE. (a) Data plots from channel 1 equipped with an FID to detect CO; (b) Data plots from channel 2 equipped with a TCD to detect H<sub>2</sub> and CH<sub>4</sub>.

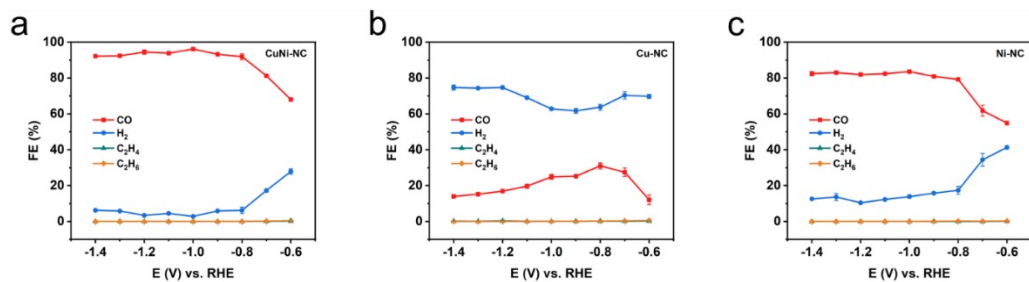


**Fig. S16** Faradaic efficiency of (a) CuNi-NC, (b) Ni-NC, and (c) Cu-NC at various applied potentials.

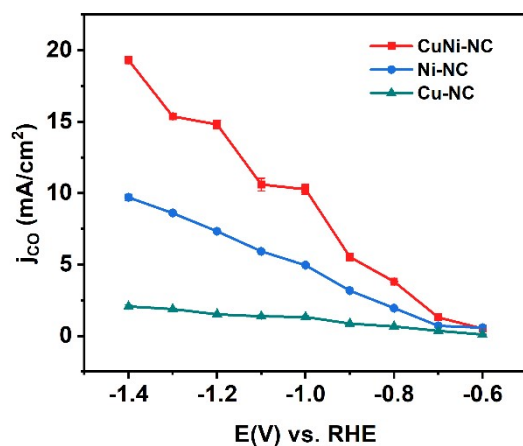


**Fig. S17** Partial current density of CO production for CuNi-NC, Ni-NC and Cu-NC.

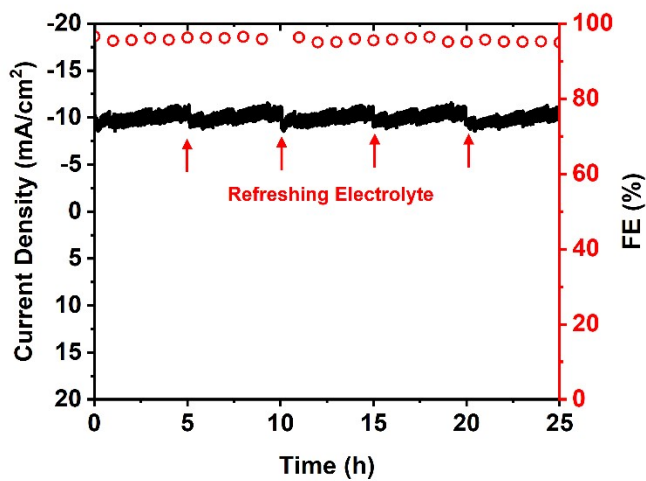


**Fig. S18** Stability test of CuNi-NC at -1.0 V vs RHE. The red arrows in the figure indicate regular refreshing of the electrolyte to eliminate the effect of the microenvironment and evaluate the intrinsic stability of CuNi-NC.

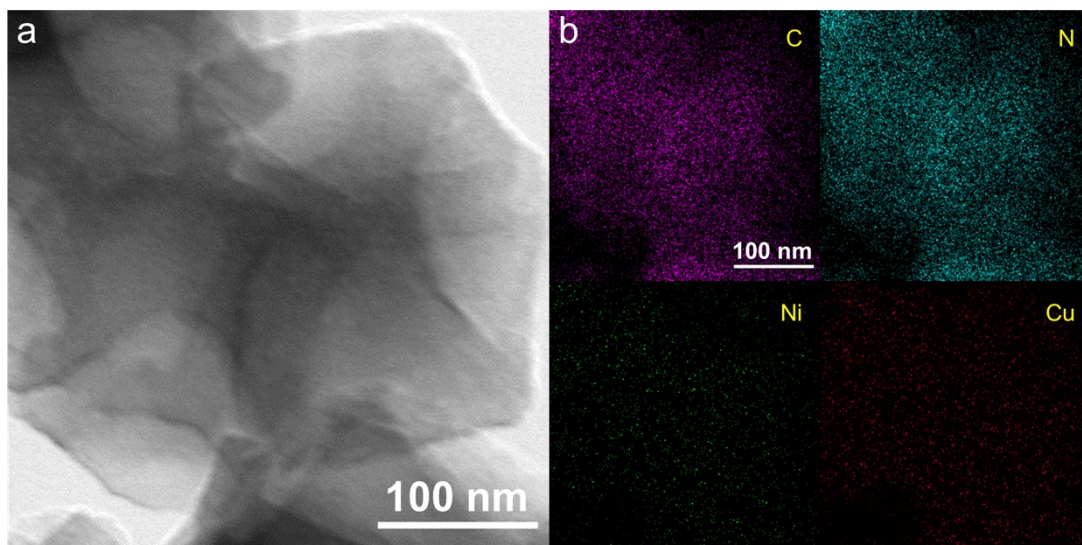


**Fig. S19** (a) TEM image of CuNi-NC after stability test and (b) corresponding elemental mapping.

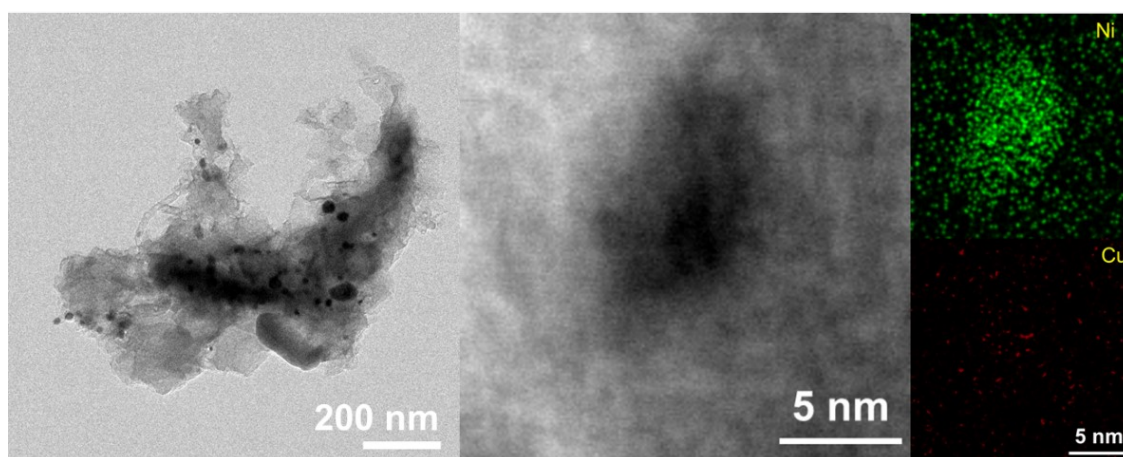


**Fig. S20** TEM image of Ni particles found in CuNi-NC after a stability test, which may be the reason for irreversible degradation due to the dissolution-deposition of catalysts.

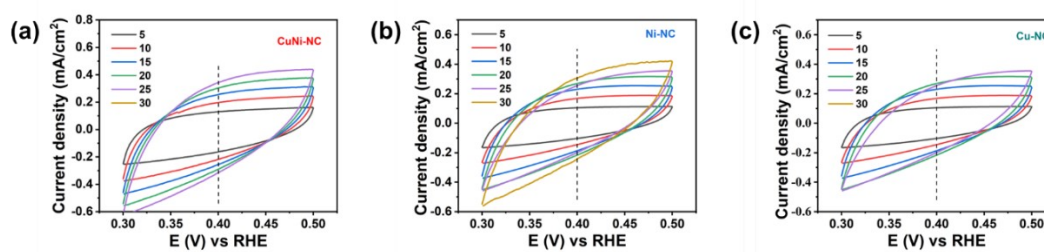


**Fig. S21** CV curves taken over a range of scan rates (5-30 mV/s) in a potential window (0.3-0.5 V vs. RHE) to measure the double-layer capacitance of (a) CuNi-NC, (b) Ni-NC and (c) Cu-NC.

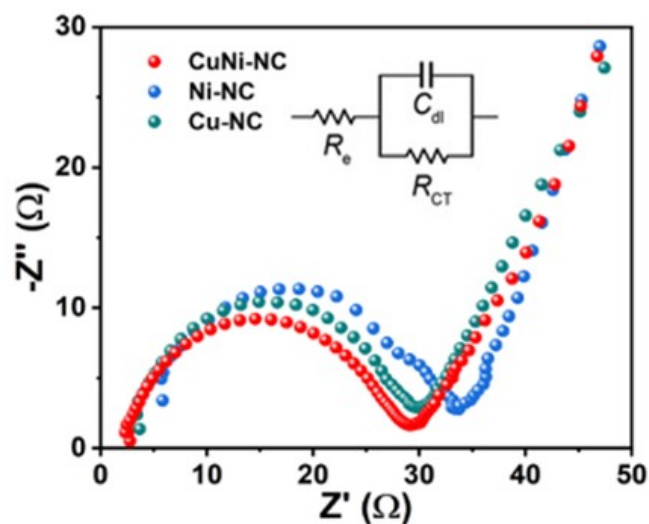


Fig. S22 Nyquist plots of CuNi-NC, Ni-NC and Cu-NC (inset: equivalent circuit).

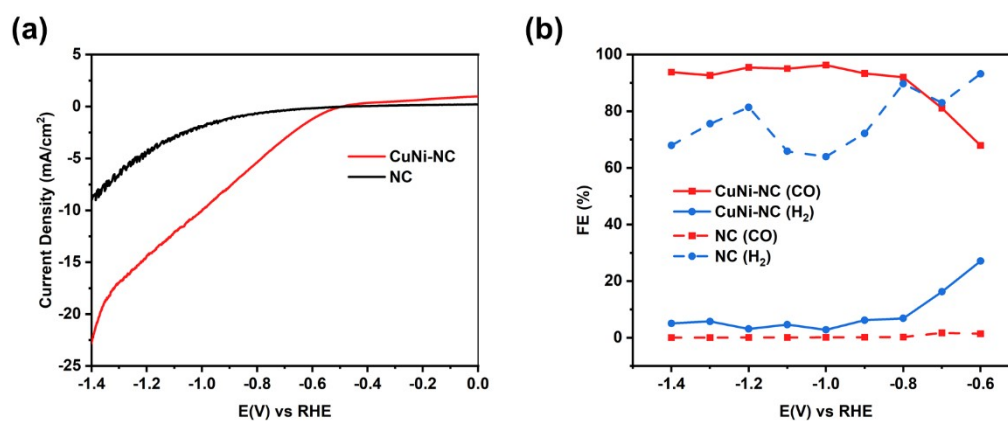


Fig. S23 ECR performance comparisons between CuNi-NC and metal-free NC. (a) LSV curves; (b) CO and H<sub>2</sub> Faradaic efficiency. The metal-free NC was synthesized by direct pyrolysis of ZIF-8 following the same time and temperature as those for CuNi-NC.

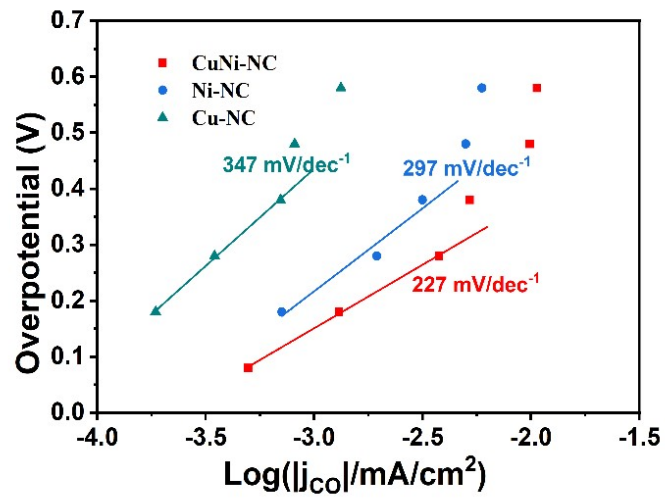


Fig. S24 Tafel plots for producing CO in CuNi-NC, Ni-NC, and Cu-NC.

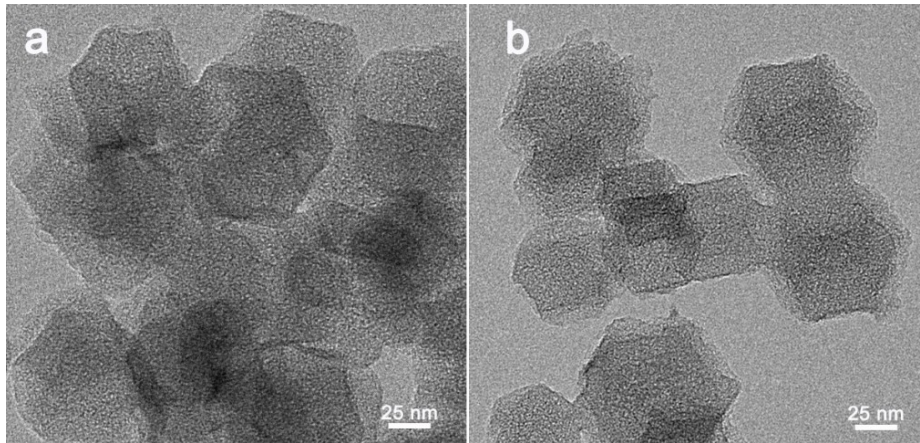


Fig. S25 TEM image of (a) CuNi-NC-0.5h, (b) CuNi-NC-1h.

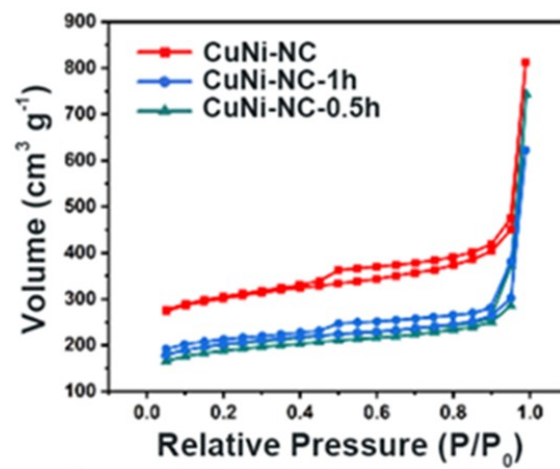


Fig. S26 N<sub>2</sub> adsorption isotherms of CuNi-NC with different pyrolysis times.

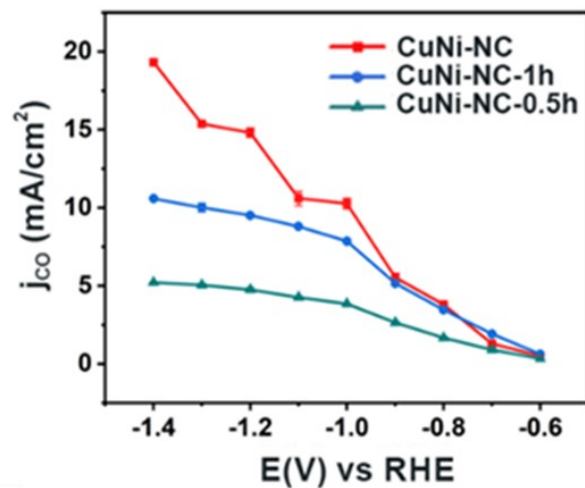


Fig. S27 Partial current density of CO production for CuNi-NC with different pyrolysis times.

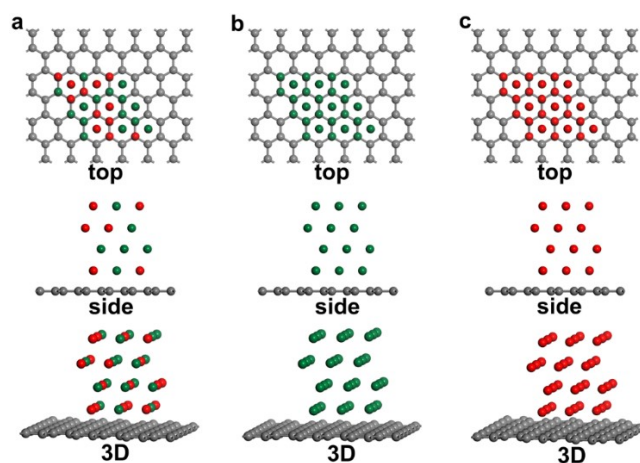


Fig. S28 The atomic slab models in the top, side, and 3D view of (a) CuNi-NC, (b) Ni-NC, and (c) Cu-NC.

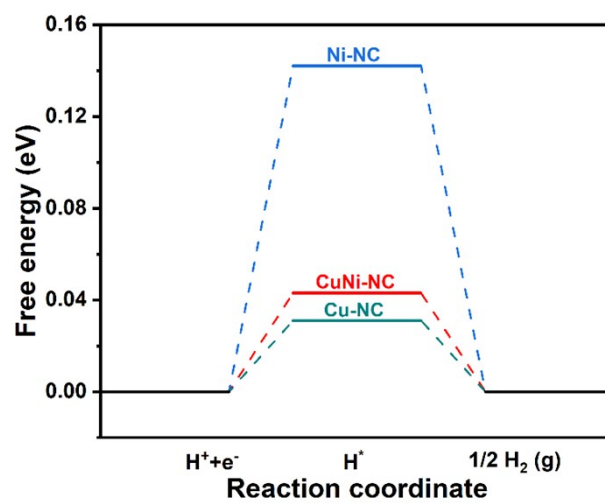


Fig. S29 Calculated Gibbs free energy diagrams for HER on CuNi-NC, Ni-NC, and Cu-NC, respectively.

**Table S1.** Elemental composition of the catalysts from ICP results.

Sample	Ni (wt%)	Cu (wt%)
CuNi-NC	1.804	1.615
Ni-NC	3.318	\
Cu-NC	\	3.557

**Table S2.** The ECR performance comparison of various catalysts.

Catalyst	Electrolyte	FE <sub>CO</sub>	j <sub>CO</sub> (mA cm <sup>-2</sup> )	Potential range (FE>90 %)	Ref.
CuNi-NC	0.1 M KHCO <sub>3</sub>	96.3% (-1.0 V)	9.86	0.6V	Our work
Fe-Nx	0.5 M KHCO <sub>3</sub>	86.9% (-0.47 V)	~3	None	11
Ni/Fe-N-C	0.5 M KHCO <sub>3</sub>	98.0% (0.7 V)	9.5	0.4 V	12
Cu SAs/NC	0.1 M KHCO <sub>3</sub>	92.0% (-0.7 V)	~3.8	0 V	13
Fe/Co-N	0.1 M KHCO <sub>3</sub>	93.0% (-0.47 V)	2.8	0 V	14
Co-PMOF	0.5 M KHCO <sub>3</sub>	98.7% (-0.8 V)	18.08	0.2 V	15
C-Zn <sub>x</sub> Ni <sub>y</sub> ZIF-8	1 M KHCO <sub>3</sub>	97.8% (-0.63 V)	N/A	0.5 V	16
FeN <sub>4</sub> /graphitic	0.1 M NaHCO <sub>3</sub>	97.0% (-0.6 V)	6.87	0.5 V	17
Ni/NC	0.1 M KHCO <sub>3</sub>	92.3% (-0.8 V)	~4	0 V	18
Cu-N <sub>4</sub>	0.1 M KHCO <sub>3</sub>	98.0% (-0.9 V)	~6	0.5 V	19
Co-N <sub>5</sub>	0.2 M NaHCO <sub>3</sub>	99.0% (-0.73 V)	4.5	0.31 V	20
Ni SAs/N-C	0.5 M KHCO <sub>3</sub>	71.9% (-0.89 V)	7.54	None	21
Ag <sub>15</sub>	0.5 M KHCO <sub>3</sub>	95.0% (-0.6V)	~2.5	0.3V	22
Au <sub>28</sub> -S	0.5 M KHCO <sub>3</sub>	98.5% (-0.9V)	~9.6	0V	23

Note:

1. The potential in FE<sub>CO</sub> is relative to RHE (V vs. RHE)
2. In the column of 'potential range', 'None' means the highest FE for CO production is less than 90%, and '0 V' means there is only one potential where FE for CO is above 90%

## Referenece

1. P. E. Blöchl, *Physical Review B*, 1994, **50**, 17953-17979.
2. G. Kresse and J. Hafner, *Physical Review B*, 1993, **47**, 558-561.
3. G. Kresse and J. Furthmüller, *Physical Review B*, 1996, **54**, 11169-11186.
4. J. P. Perdew, J. A. Chevary, S. H. Vosko, K. A. Jackson, M. R. Pederson, D. J. Singh and C. Fiolhais, *Physical Review B*, 1992, **46**, 6671-6687.
5. T. Zhang, X. Han, H. Yang, A. Han, E. Hu, Y. Li, X.-q. Yang, L. Wang, J. Liu and B. Liu, *Angew. Chem. Int. Ed.*, 2020, **59**, 12055-12061.
6. H. J. Monkhorst and J. D. Pack, *Physical Review B*, 1976, **13**, 5188-5192.
7. H. Mistry, R. Reske, Z. Zeng, Z.-J. Zhao, J. Greeley, P. Strasser and B. R. Cuenya, *J. Am. Chem. Soc.*, 2014, **136**, 16473-16476.
8. W. Zhu, Y.-J. Zhang, H. Zhang, H. Lv, Q. Li, R. Michalsky, A. A. Peterson and S. Sun, *J. Am. Chem. Soc.*, 2014, **136**, 16132-16135.
9. B. Hinnemann, P. G. Moses, J. Bonde, K. P. Jørgensen, J. H. Nielsen, S. Horch, I. Chorkendorff and J. K. Nørskov, *J. Am. Chem. Soc.*, 2005, **127**, 5308-5309.
10. J. K. Nørskov, T. Bligaard, A. Logadottir, J. R. Kitchin, J. G. Chen, S. Pandalov and U. Stimming, *J. Electrochem. Soc.*, 2005, **152**, J23.
11. X. Chen, D.-D. Ma, B. Chen, K. Zhang, R. Zou, X.-T. Wu and Q.-L. Zhu, *Appl. Catal., B*, 2020, **267**, 118720.
12. W. Ren, X. Tan, W. Yang, C. Jia, S. Xu, K. Wang, S. C. Smith and C. Zhao, *Angew. Chem. Int. Ed.*, 2019, **58**, 6972-6976.
13. F. Yang, X. Mao, M. Ma, C. Jiang, P. Zhang, J. Wang, Q. Deng, Z. Zeng and S. Deng, *Carbon*, 2020, **168**, 528-535.
14. F. Pan, H. Zhang, K. Liu, D. Cullen, K. More, M. Wang, Z. Feng, G. Wang, G. Wu and Y. Li, *ACS Catal.*, 2018, **8**, 3116-3122.
15. Y.-R. Wang, Q. Huang, C.-T. He, Y. Chen, J. Liu, F.-C. Shen and Y.-Q. Lan, *Nat. Commun.*, 2018, **9**, 4466.
16. C. Yan, H. Li, Y. Ye, H. Wu, F. Cai, R. Si, J. Xiao, S. Miao, S. Xie, F. Yang, Y. Li, G. Wang and X. Bao, *Energy Environ. Sci.*, 2018, **11**, 1204-1210.
17. C. Liu, Y. Wu, K. Sun, J. Fang, A. Huang, Y. Pan, W.-C. Cheong, Z. Zhuang, Z. Zhuang, Q. Yuan, H. L. Xin, C. Zhang, J. Zhang, H. Xiao, C. Chen and Y. Li, *Chem*, 2021, **7**, 1297-1307.
18. F. Li, S. Hong, T.-S. Wu, X. Li, J. Masa, Y.-L. Soo and Z. Sun, *ACS Appl. Energy Mater.*, 2019, **2**, 8836-8842.
19. H. Cheng, X. Wu, X. Li, X. Nie, S. Fan, M. Feng, Z. Fan, M. Tan, Y. Chen and G. He, *Chem. Eng. J.*, 2021, **407**, 126842.
20. Y. Pan, R. Lin, Y. Chen, S. Liu, W. Zhu, X. Cao, W. Chen, K. Wu, W.-C. Cheong, Y. Wang, L. Zheng, J. Luo, Y. Lin, Y. Liu, C. Liu, J. Li, Q. Lu, X. Chen, D. Wang, Q. Peng, C. Chen and Y. Li, *J. Am. Chem. Soc.*, 2018, **140**, 4218-4221.
21. C. Zhao, X. Dai, T. Yao, W. Chen, X. Wang, J. Wang, J. Yang, S. Wei, Y. Wu and Y. Li, *J. Am. Chem. Soc.*, 2017, **139**, 8078-8081.
22. L. Qin, F. Sun, X. Ma, G. Ma, Y. Tang, L. Wang, Q. Tang, R. Jin and Z. Tang, *Angew. Chem. Int. Ed.*, 2021, **60**, 26136-26141.
23. J. Wang, F. Xu, Z.-Y. Wang, S.-Q. Zang and T. C. W. Mak, *Angew. Chem. Int. Ed.*, 2022, **61**, e202207492.

**Author Contributions**

J. Wang and J. Wu conceived the idea and designed the experiments, J. Wang carried out the synthesis, characterization, and electrochemical performance evaluation of the catalysts, F. Li carried out the DFT calculations. J. Wang and R. Li analyzed the data and wrote the paper. Q. Xiang and W. Zhang developed the methodology. J. Wu supervised the investigation during the whole project. All the authors contributed to the discussions. All authors discussed the results and commented on the manuscript.